Supplementary Information

Eliminating high-dimensional defects by upward unidirectional crystallization for efficient and stable inverted perovskite solar cells

Zhenzhen Qin[a], Mengjiong Chen[a], Ziyang Zhang[a], Yanbo Wang[a]*, Liyuan Han[a]*

[a] State Key Laboratory of Metal Matrix Composites, Shanghai Jiao Tong University, 800 Dong Chuan Road, Shanghai 200240, China.

*Corresponding author. Email: sjtu-wyb@sjtu.edu.cn; han.liyuan@sjtu.edu.cn

Materials

Nickel (II) oxide nanoparticle powder (particle size around 10 nm) was purchased from Advanced Election Technology Co., Ltd. Ethanol absolute (99.5%), deionized water, dimethylformamide (DMF, 99.9%), dimethyl sulfoxide (DMSO, 99.9%), 2-propanol (IPA, 99.5%) and chlorobenzene (CB, 99.8%) were purchased from Sigma Aldrich. [4-(3,6-dimethyl-9H-carbazol-9-Yl) butyl] phosphonic acid (Me-4PACz, 99%), lead iodide (PbI_2, 98%), lead bromide ($PbBr_2$, 98%), formamidinium iodide (FAI, 98%), cesium iodide (CsI, 99%), methylammonium chloride (MACl, 98%) and methylamine hydrobromide (MAI, 99%) were purchased from Tokyo Chemical Industry. Bathocuproine (BCP, 99.5%) and $CsPbBr_3$ (99%) were purchased from Xi'an Yuri Solar Co., Ltd. 4-Fluoro-2-methylbenzonitrile (FMeB, 98%) and 4-Fluoro-2-methoxybenzonitrile (FMeOB, 97%) were purchased from Adamas. [6,6]-phenyl-C61-butyric acid methyl ester (PCBM, 99.5%) was purchased from Luminescence technology corp. All the chemicals are used directly without further purification.

Normal-bandgap Perovskite Solar Cell Fabrication

Indium tin oxide (ITO) glass substrates were cleaned by sequentially ultrasonication with detergent, deionized water, ethanol absolute, acetone and IPA, each for 15 minutes. Before use, the ITO was cleaned with ultraviolet ozone for 20 minutes. The NiO_x (5 mg/mL) dissolved in deionized water was deposited on the ITO substrate by spin-coating at 3000 rpm for 30 seconds and annealing at 150 ℃ for 20 minutes in air. Then the substrates were quickly transferred to a N_2 filled glove box for subsequent deposition. 0.5 mg/ml Me-4PACz dissolved in ethanol absolute was spin-coated on NiO_x at 4000 rpm for 30 seconds, followed by annealing at 100 ºC for 10 minutes. For the pristine perovskite sample, 1.4 M perovskite precursor solution was prepared by mixing CsI, FAI, MAI, $PbBr_2$ and PbI_2 in DMF:DMSO (4:1/v:v) mixed solvent with chemical formula of $Cs_{0.05}(FA_{0.95}MA_{0.05})_{0.95}Pb(I_{0.98}Br_{0.02})_3$. 5 mol% of excess PbI_2 was needed to improve the device performance. Then, 12 mol% MACl was added to the

perovskite precursor solution and stirred for 2 h. For the bottom-side treated (BST) and double-side treated (DST) perovskite sample, 2% $CsPbBr_3$-seed dissolved in DMSO was added to the perovskite precursor solution to substitute for part of the CsI and all of the $PbBr_2$. Perovskite solutions were deposited by a two-step spin-coating of 1000 rpm for 10 seconds and 5000 rpm for 30 seconds. For the pristine and BST perovskite deposition, 150 μL CB was slowly dripped onto the center of film at 15 seconds before the end of spin-coating. For the DST perovskite deposition, 150 μL FMeB or FMeOB solution (0.5-2 mg/mL in CB) was employed as the antisolvent and was used in the same way. The as-prepared perovskite films were subsequently annealed on a hotplate at 100 ^oC for 20 minutes. Then, 20 mg/ml of PCBM dissolved in CB was spin-coated at 1000 rpm for 30 seconds, followed by annealing at 70 ^oC for 10 minutes. 0.5 mg/ml of BCP dissolved in IPA was spin-coated at 6000 rpm for 30 seconds, followed by annealing at 70 ^oC for 10 minutes. Finally, 90 nm thickness of Ag was thermally evaporated as an electrode using a shadow mask with aperture area of 0.0795 cm^2. After finishing the device fabrication, 120 nm thickness of MgF_2 anti-reflection coatings were made on the glass side of the ITO substrate via thermal evaporation.

Wide-bandgap Perovskite Solar Cell Fabrication

The HTL deposition was the same as normal-bandgap PSCs. For the pristine perovskite sample, 1.1 M perovskite precursor solution was prepared by mixing CsI, FAI, $PbBr_2$ and PbI_2 in DMF:DMSO (4:1/v:v) mixed solvent with chemical formula of $Cs_{0.2}FA_{0.8}PbI_{1.9}Br_{1.1}$. 12 mol% MACl and extra 5 mol% PbI_2 were added into the perovskite precursor solution and stirred for 2 hours to improve the device performance. For DST perovskite sample, 2% $CsPbBr_3$-seed dissolved in DMSO was added to the perovskite precursor solution to substitute for part of the CsI and the $PbBr_2$. Perovskite solutions were deposited by a two-step spin-coating of 1000 rpm for 10 seconds and 4500 rpm for 30 seconds. For the pristine perovskite deposition, 150 μL CB was slowly dripped onto the center of film at 15 seconds before the end of spin-coating. For the

DST perovskite deposition, 150 μL FMeOB solution (1.0 mg/mL in CB) was employed as the antisolvent and was used in the same way. The as-prepared perovskite films were subsequently annealed on a hotplate at 100 ^{o}C for 20 minutes. The PCBM, BCP, Ag and MgF_2 deposition were the same as normal-bandgap PSCs.”

Characterization of materials

Scanning electron microscope (SEM) images were measured by JSM-7800F (JEOL, China). For the lift-off process for SEM characterization, the perovskite film deposited on NiO_x/SAM substrate is encapsulated with UV Epoxy and a cover glass. After complete solidification of UV Epoxy, the perovskite film adhered to the cover glass with an exposed buried surface can be obtained by separating the cover glass from NiO_x/SAM substrate. The time-of-flight secondary ion mass spectroscopy was performed with an IONTOF TOF.SIMS 5-100 instrument. Ar cluster (10 keV) was used in the sputtering and Bi^{3+} (30 keV) was used to probe the sample with an analysis area of $100 \times 100\ \mu m^2$. Grazing-incidence wide-angle X-ray scattering (GIWAXS) measurement was measured at beamline BL17B1 at Shanghai Synchrotron Radiation Facility (SSRF). Atomic force microscope (AFM) and Kelvin probe force microscopy (KPFM) were measured by Dimension XR (Bruker). X-ray photoelectron spectroscopy (XPS) and ultraviolet photoelectron spectroscopy (UPS) were measured by AXIS Ultra DLD (China) with an Al Kα X-ray source and He Iα photon source (21.2 eV) respectively. Fourier transform infrared (FTIR) spectra was measured by Nicolet 6700 (THERMO FISHER, USA). ^{1}H NMR spectra was characterized by Avance III (Bruker Co., Germany). For NMR measurement, the perovskite films were scraped from the glass substrates with a stainless-steel blade. Then, the scraped powder was transferred into the NMR tube containing 0.5 mL D_2O followed by an ultrasonic treatment for 30 minutes. Grazing incidence X-ray diffraction (GIXRD) patterns were measured by X-Ray diffractometer (D8 ADVANCE Da Vinci) using Cu Kα radiation. X-ray diffraction

(XRD) patterns were measured by Mini Flex 600 (Rigaku, Japan) using Cu Kα radiation. UV-visible absorption spectra was measured by Shimadzu UV 2450 spectrometry.

Characterization of devices

Current density-voltage (*J-V*) curves of PSCs were measured by a Keithley 2400 digital source meter under a simulated solar source of AM 1.5G (100 mW cm^{-2}, Wacom Denso Co., Japan). The measurement was conducted under forward (from -0.1 to 1.3 V) scan or reverse (from 1.3 to -0.1 V) scan. The delay time and step voltage were set as 20 ms and 20 mV, respectively. The incident photon-to-electron conversion efficiency (IPCE) spectra were performed with director current mode (CEP-2000BX, Bunko-Keiki). For the ideality factors measurement, light intensity-dependent *J-V* curves were measured under different light intensities (1, 5, 10, 20, 30, 40, 50, 60, 70, 80, 90, 100 mW cm^{-2}) controlled by filters with different transmittance to obtain relevant V_{OC}. The dark current, thermal admittance spectroscopy (TAS) and drive-level capacitance profiling (DLCP) were performed on Zahner, Germany. The transient photovoltage (TPV) and transient photocurrent (TPC) tests were performed on an attenuated UV laser pulse (SRS NL 100 Nitrogen Laser) under 1 sun illumination. The laser wavelength is 337 nm, the repeating frequency was about 20 Hz, and the pulse width was less than 3.5 ns.

Device stability test

Long-term operational stability measurements of encapsulated PSCs devices were operated under a white LED light with 1 sun equivalent intensity and the temperature is controlled to be ~65 °C. The perovskite solar cells were encapsulated with UV-curable epoxy and a glass coverslip in N_2-filled glove box. All devices were loaded with a resistance so that they worked at maximum power point (MPP) at the beginning of the tests. The *J-V* curves were automatically recorded with reverse scan rate of 0.1 V s^{-1} every 12 hours. Damp-heat stability measurements were keeping the devices in

85 °C/85% RH test chamber. Before *J-V* measurement, the devices were taken out and were measured until cooling down to room temperature.

Quantum chemical calculations

For the calculation of electrostatic potential, the geometry structure of molecules was optimized in the gas phase, followed by employing B3LYP as the exchange-correlation function and def2TZVP basis sets. The calculation was performed on Gaussian 09 program and the output files were visualized by GaussView 5.0. For the interaction between PbI_2 and molecules, single point calculations were performed for both FMeB and FMeOB molecules with PbI_2. Then, using Multiwfn software combined with VMD program, the IRI method was used to graphically investigate chemical bonds and weak interactions in the chemical system, and finally the visualization was achieved.

First-principles density functional theory (DFT) was used as implemented in the Vienna Ab initio simulation package (VASP). The exchange-correlation potential is described by using the generalized gradient approximation of Perdew-Burke-Ernzerhof (GGA-PBE). The projector augmented-wave (PAW) method is employed to treat interactions between ion cores and valence electrons. The plane-wave cutoff energy was fixed to 400 eV. A Monkhorst-Pack k-mesh with a 2 × 2 × 1 k-point grid was used for structural optimization. The structural models were relaxed until the Hellmann-Feynman forces smaller than -0.02 eV/Å and the change in energy smaller than 10^{-5} eV was attained. The long-range van der Waals interaction is described by the DFT-D3 approach.

The adsorption energy (*E*ads) of species is calculated by:

$$E\text{ads} = E(\text{system}) - E(\text{catalyst}) - E(\text{species})$$

where *E*(system), *E*(catalyst), and *E*(species) are the total energy of the optimized system with adsorbed species, the isolated catalyst, and species, respectively.

Supplementary Note 1

The charge density distribution derived from KPFM[1]

The real-time electric field, $E(x)$, across the perovskite device cross section under illumination can be derived from the contact potential distribution (CPD) as:

$$-\frac{\mathrm{d}}{\mathrm{d}x}\mathrm{CPD}(x) = -\frac{\mathrm{d}}{\mathrm{d}x}\left[V_{\mathrm{E}}(x) - \frac{1}{e}\Phi_{tip}(x)\right] = E(x)$$

where $V_{\mathrm{E}}(x)$ is the local electric potential of the surface underneath of the probe, and $\Phi_{tip}(x)$ is the work function of the probe, which remains unchanged during the measurement. The local charge density $\rho(x)$ is then given by:

$$\rho(x) = \varepsilon_0\varepsilon_r\frac{\mathrm{d}}{\mathrm{d}x}E(x)$$

where ε_0 and ε_r are the vacuum and relative permittivity, respectively.

Supplementary Note 2

tDOS and DLCP measurements[2]

For thermal admittance spectroscopy (TAS), a steady DC bias of 0 V was maintained with the AC bias amplitude of 20 mV, and the AC frequency dependence of the capacitance was recorded from 10 Hz to 10 MHz. The tDOS ($N_T(E_\omega)$) is derived from the capacitance-frequency C-f spectrum according to the following equation:

$$N_T(E_\omega) = -\frac{1}{qk_{\mathrm{B}}T}\frac{\omega\mathrm{d}C}{\mathrm{d}\omega}\frac{V_{\mathrm{bi}}}{W}$$

where V_{bi} and W are built-in potential and depletion width, respectively, determined through Mott-Schottky curves derived from C-V measurement. ω, q, k_{B} and T denote angular frequency, elementary charge, Boltzmann constant and temperature, respectively. The correlation between applied ω and energetic demarcation is given as follows:

$$E_\omega = k_{\mathrm{B}}T\ln\frac{\omega}{\omega_0}$$

where ω_0 is the attempt-to escape angular frequency:

$$\omega_0 = 2\pi v_0 T^2$$

where v_0 denotes the temperature-independent attempt-to escape frequency, derived from temperature-dependent C-f measurement.

For the DLCP measurement, the DC bias was set from 0 to 1.3 V at different AC bias (dV) from 20 to 200 mV, with an AC scanning frequency of 100 kHz, related to defects at shallow energy levels. The capacitance measured at each dV can be fitted to obtain $C_0$and C_1 according to the following formula:

$$C = C_0 + C_1 dV + C_2 dV^2 + \cdots$$

The trap density (N_T) can be calculated as follows:

$$N_T = -\frac{C_0^3}{2q\varepsilon_0\varepsilon_r A^2 C_1}$$

where A denotes the active area. The profiling distance (X) can be obtained according to the follow formula:

$$X = \varepsilon_0\varepsilon_r \frac{A}{C_0}$$

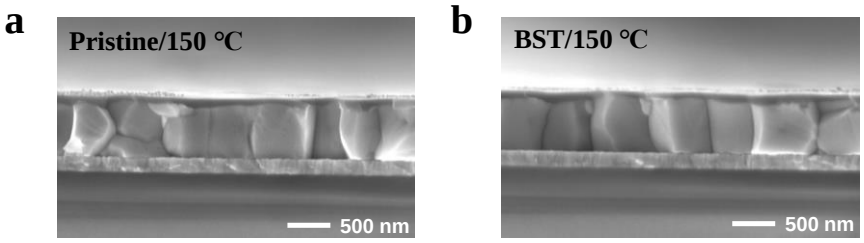

Figure S1. Cross-sectional SEM images for PSCs based on (a) pristine and (b) BST perovskite films annealing at 150 °C.

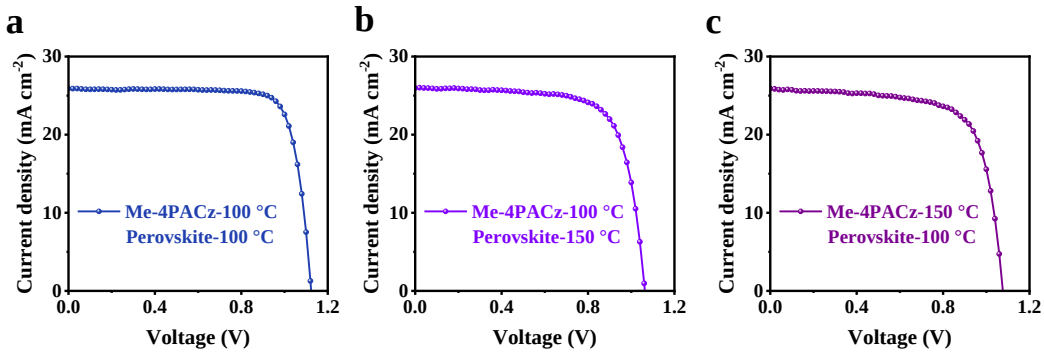

Figure S2. *J-V* curves of devices based on Me-4PACz and perovskite films annealing at different temperature.

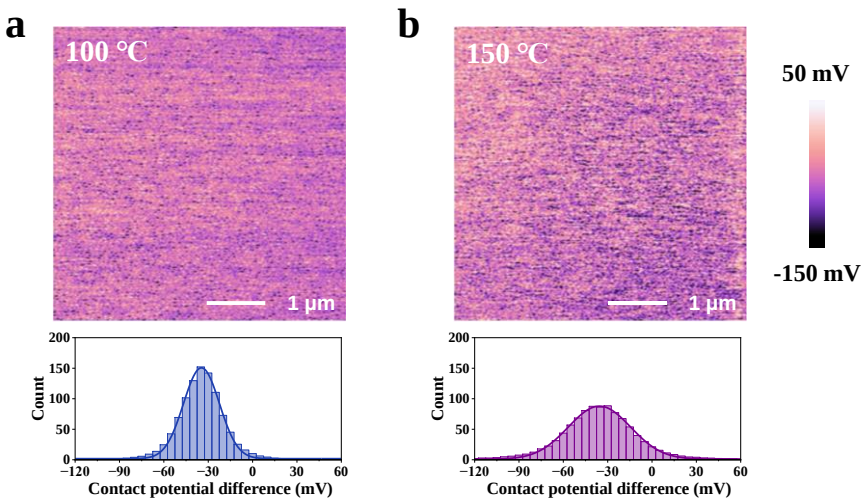

Figure S3. Surface potential distribution of Me-4PACz annealing at (a) 100 ^{o}C and (b) 150 ^{o}C for 10 minutes, respectively, measured by KPFM.

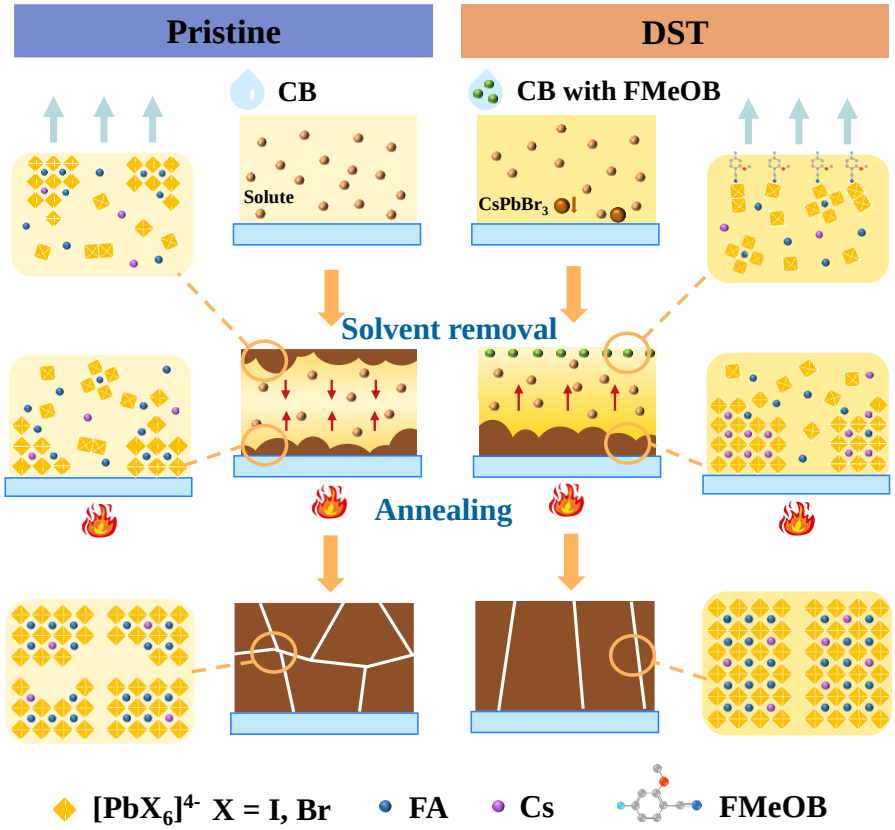

Figure S4. Illustration of nucleation and growth of perovskite grains in pristine and DST strategy.

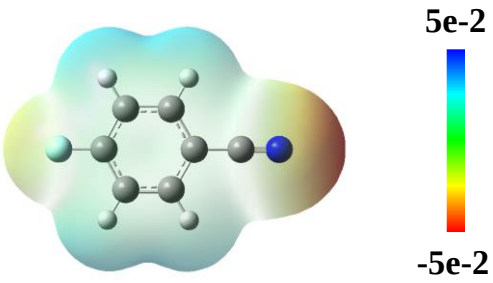

Figure S5. Electrostatic potential images of 4-Fluorobenzonitrile.

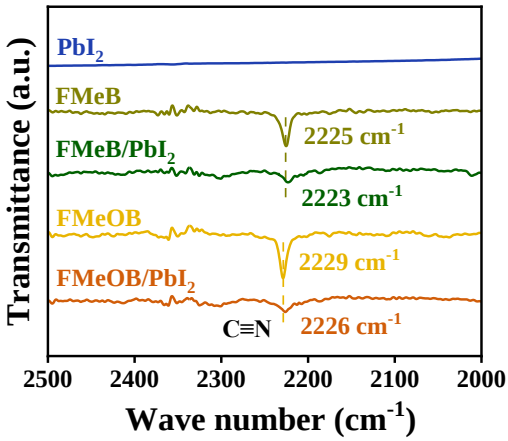

Figure S6. FTIR spectra of PbI_2, FMeB, PbI_2-FMeB, FMeOB and PbI_2-FMeOB.

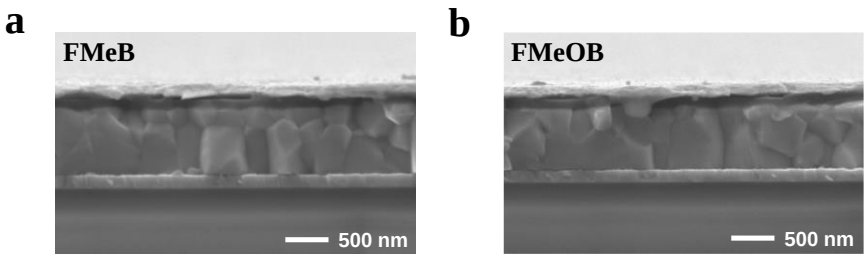

Figure S7. Cross-sectional SEM images for complete devices based on (a) FMeB-treated and (b) FMeOB-treated perovskite films.

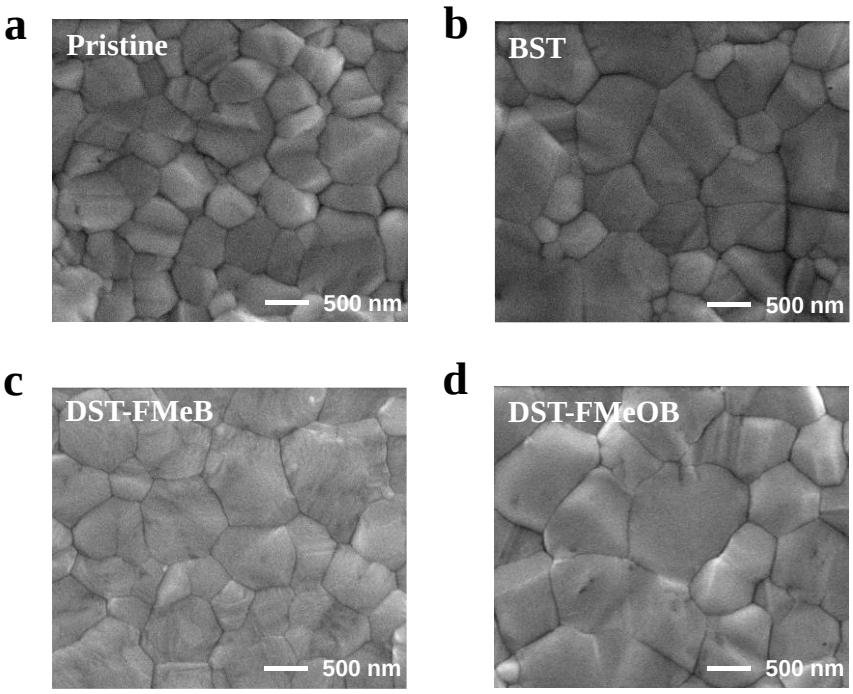

Figure S8. Top-view SEM images of (a) pristine, (b) BST, (c) DST-FMeB and (d) DST-FMeOB perovskite films.

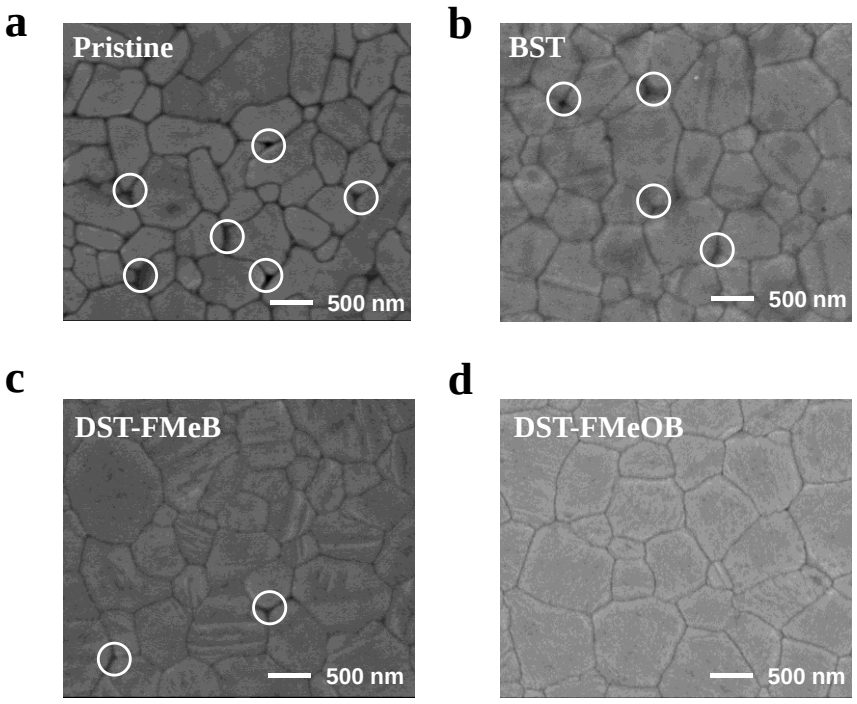

Figure S9. Top-view SEM images for the buried surface of (a) pristine, (b) BST, (c) DST-FMeB and (d) DST-FMeOB perovskite films.

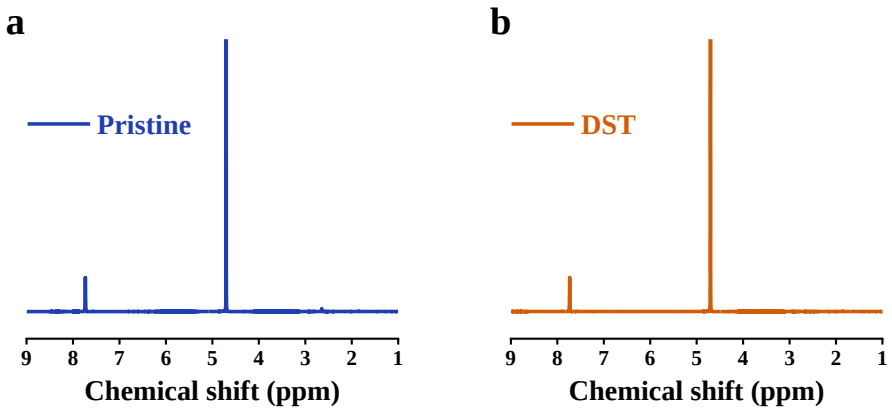

Figure S10. ^{1}H NMR spectra of (a) pristine and (b) DST-FMeOB perovskites dissolved in D_2O. Signals at 2.65 ppm and 7.73 ppm correspond to DMSO and FA^{+}, respectively.

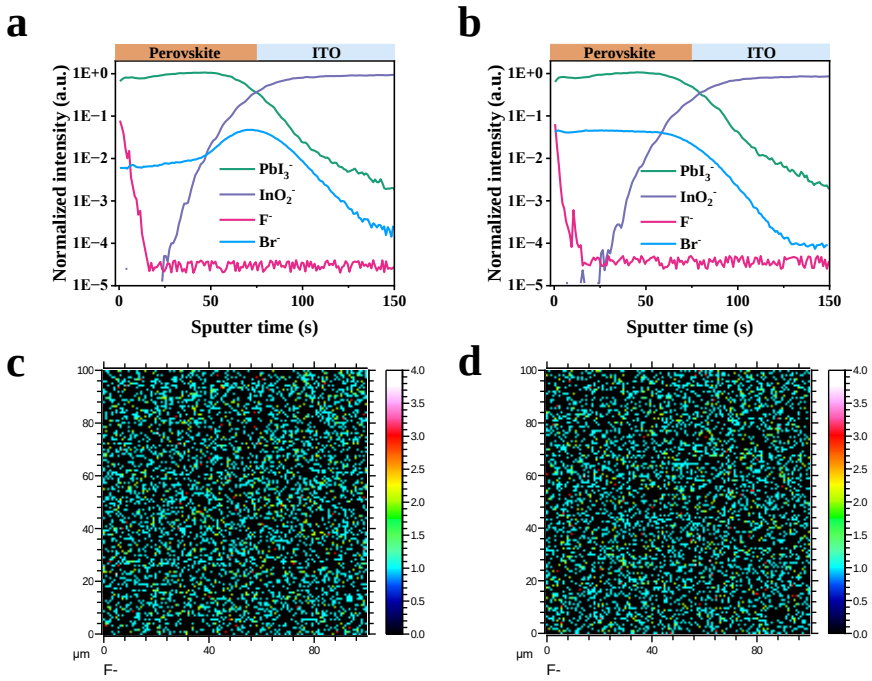

Figure S11. ToF-SIMS depth profiles of DST-FMeOB perovskite films before (a) and after (b) annealing. ToF-SIMS signal of F^- from 100 * 100 μm^2 DST-FMeOB perovskite surface before (c) and after (d) annealing.

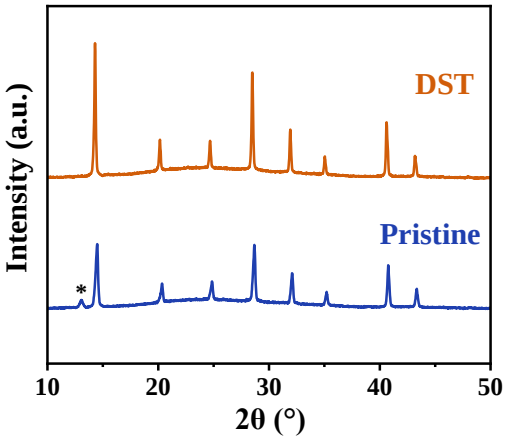

Figure S12. XRD patterns of final pristine and DST-FMeOB perovskite films. * denotes PbI_2.

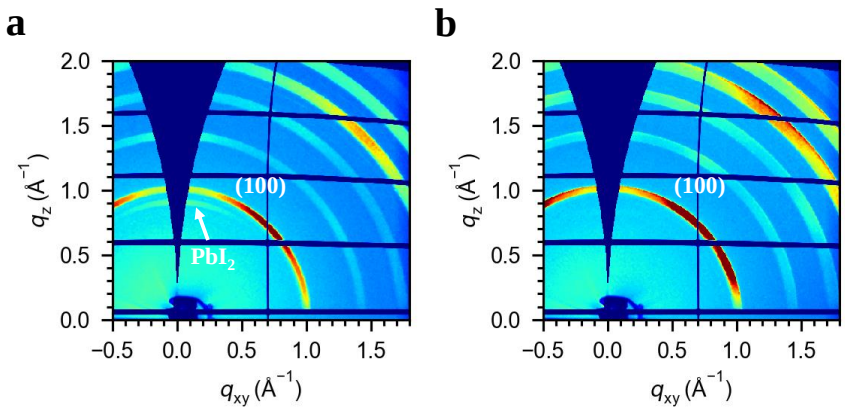

Figure S13. GIWAXS data of final (a) pristine and (b) DST-FMeOB perovskite films.

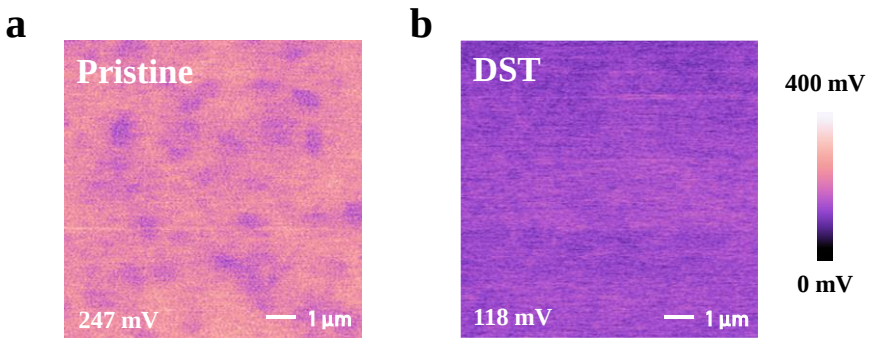

Figure S14. KPFM of the surface for (a) pristine and (b) DST-FMeOB perovskite films.

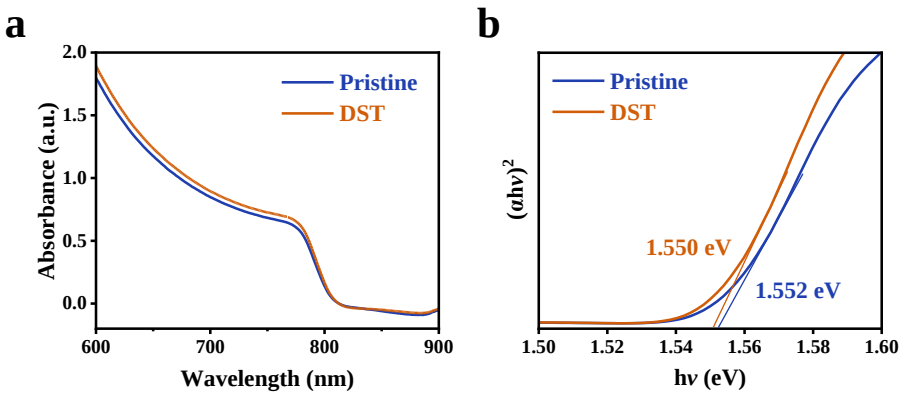

Figure S15. (a) UV-vis absorbance spectra and (b) the corresponding Tauc plots of pristine and DST-FMeOB perovskite films.

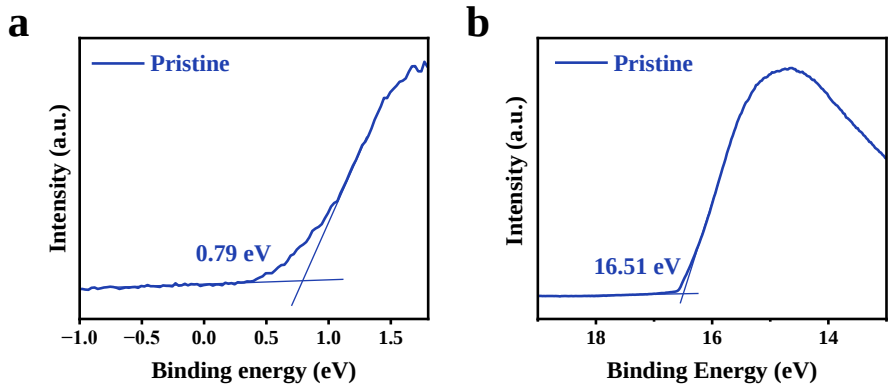

Figure S16. UPS spectra of (a) secondary electron cutoff region and (b) Fermi edge region of the pristine perovskite film.

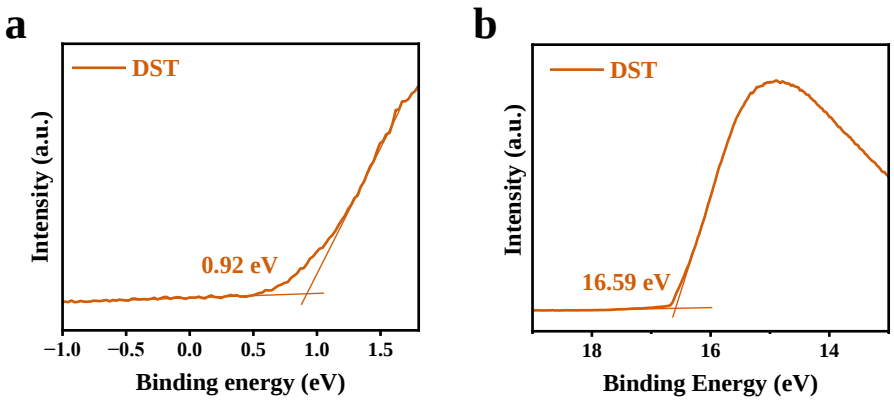

Figure S17. UPS spectra of (a) secondary electron cutoff region and (b) Fermi edge region of the DST-FMeOB perovskite film.

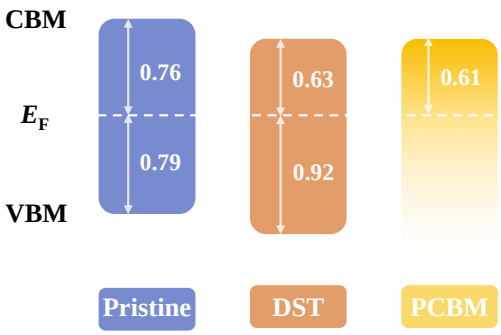

Figure S18. Schematic diagram of smooth energy-level of respective components based on pristine and DST-FMeOB perovskite as absorber layer. The energy level data for PCBM is obtained from the literature.[3]

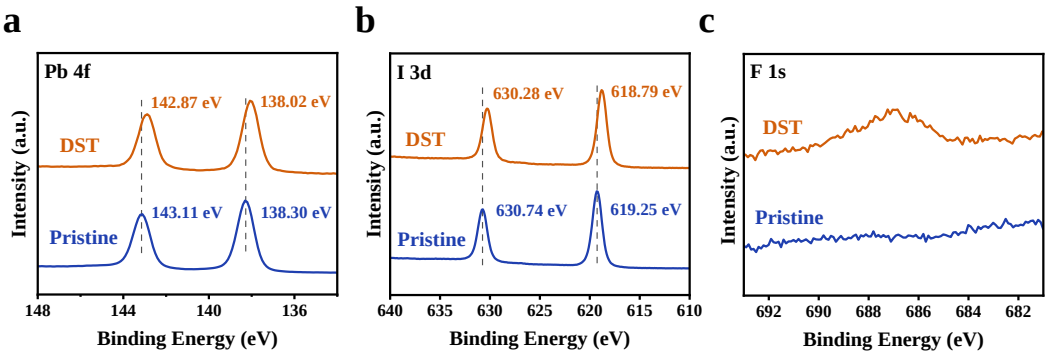

Figure S19. XPS spectra of (a) Pb 4f, (b) I 3d and (c) F 1s for pristine and DST-FMeOB perovskite films.

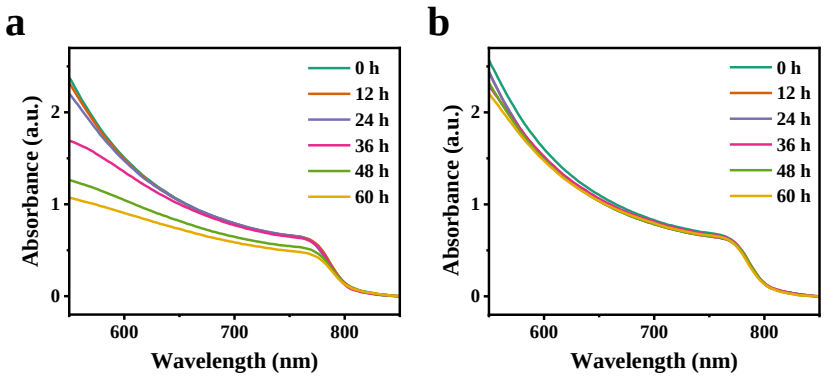

Figure S20. The evolution of UV-vis absorption curves of (a) pristine and (b) DST-FMeOB perovskite films aging at 85 ºC and 85% RH.

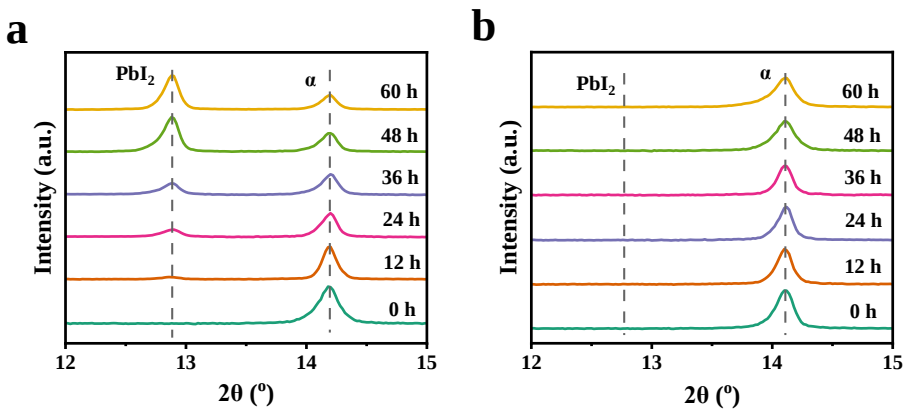

Figure S21. The evolution of XRD patterns for (a) pristine and (b) DST perovskite films aging at 85 °C and 85% RH.

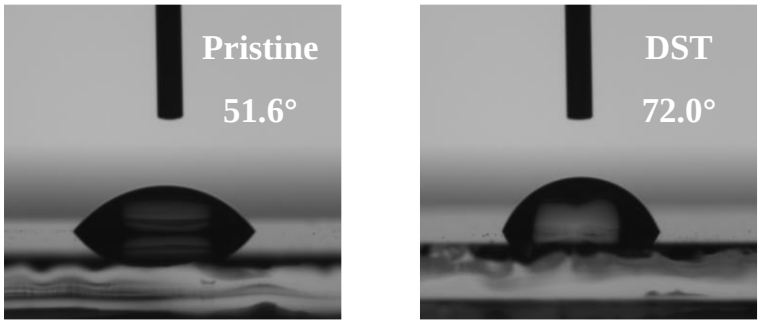

Figure S22. Water contact angle test of pristine and DST perovskite films.

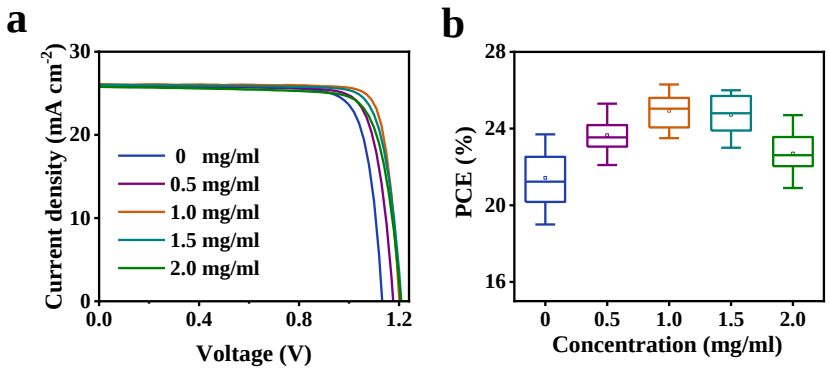

Figure S23. (a) *J-V* curves of the champion DST devices with FMeOB at different concentration in the antisolvent. (b) PCEs distribution of 20 devices for each batch.

Test and Calibration Center of New Energy Device and Module,
Shanghai Institute of Microsystem and Information Technology,
Chinese Academy of Sciences (SIMIT)

Measurement Report

Report No. 24TR092802

Client Name	Shanghai Jiao Tong University
Client Address	800 Dongchuan Road, Minhang District, Shanghai
Sample	Perovskite solar cell
Manufacturer	Shanghai Jiao Tong University
Measurement Date	28th September, 2024

Performed by:	Qiang Shi	**Date:** 28/09/2024
Reviewed by:	Wenjie Zhao	**Date:** 28/09/2024
Approved by:	Yucheng Liu	**Date:** 28/09/2024

Address: No.235 Chengbei Road, Jiading, Shanghai **Post Code:**201800
E-mail: solarcell@mail.sim.ac.cn **Tel:** +86-021-69976905

Sample Information

Sample Type	Perovskite solar cell
Serial No.	10-5-2
Lab Internal No.	24092801-2#
Measurement Item	I-V characteristic
Measurement Environment	24.8±2.0°C, 40.3±5.0%R.H

Measurement of I-V characteristic

Reference cell	PVM1121
Reference cell Type	mono-Si, WPVS, calibrated by NREL (Certificate No. ISO 2098)
Calibration Value/Date of Calibration for Reference cell	143.95mA/ Feb. 2024
Measurement Conditions	Standard Test Condition (STC): Spectral Distribution: AM1.5, Irradiance: 1000±50W/m², Temperature: 25±2°C
Measurement Equipment/ Date of Calibration	AAA Steady State Solar Simulator (YSS-T155-2M) / Sep.2023 IV test system (ADCMT 6246) / June. 2024 Measuring Microscope (MF-B2017C) / July.2024
Measurement Method	I-V Measurement: Dual-lamp solar simulator spectral distribution adjusted to make the match factor within 1.00±0.01, Irradiance adjusted to 1 Sun according to reference cell calibration value. Logarithmic sweep in both directions (Voc to Isc and Isc to Voc) during one flash based on IEC 60904-1:2020
Measurement Uncertainty	Area: 1.0%(k=2); Isc: 2.1%(k=2); Voc: 1.0%(k=2); Pmax: 2.5%(k=2); Eff: 2.6%(k=2)

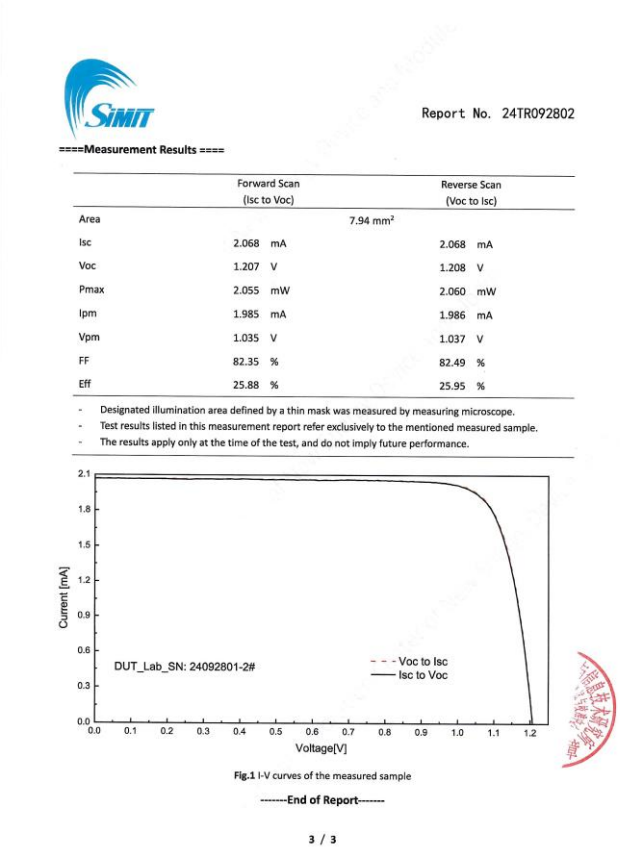

Report No. 24TR092802

====Measurement Results ====

	Forward Scan (Isc to Voc)	Reverse Scan (Voc to Isc)
Area	7.94 mm²	
Isc	2.068 mA	2.068 mA
Voc	1.207 V	1.208 V
Pmax	2.055 mW	2.060 mW
Ipm	1.985 mA	1.986 mA
Vpm	1.035 V	1.037 V
FF	82.35 %	82.49 %
Eff	25.88 %	25.95 %

- Designated illumination area defined by a thin mask was measured by measuring microscope.
- Test results listed in this measurement report refer exclusively to the mentioned measured sample.
- The results apply only at the time of the test, and do not imply future performance.

Fig.1 I-V curves of the measured sample

-------End of Report-------

3 / 3

Figure S24. Certification report of the best-performance DST device. Tested by Shanghai Institute of Microsystem and Information Technology (SIMIT), Chinese Academy of Sciences (CAS).

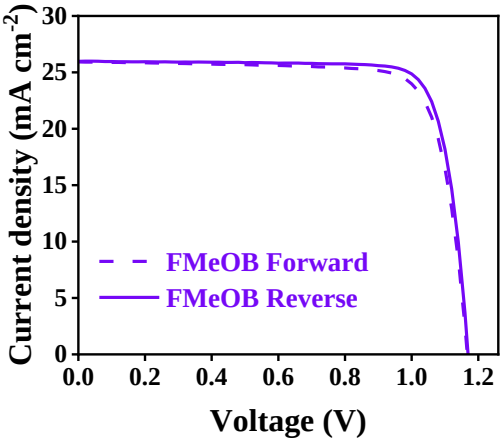

Figure S25. *J-V* curves of the champion device with the perovskite film post-treated by FMeOB. The concentration of FMeOB is 1mg/ml in CB.

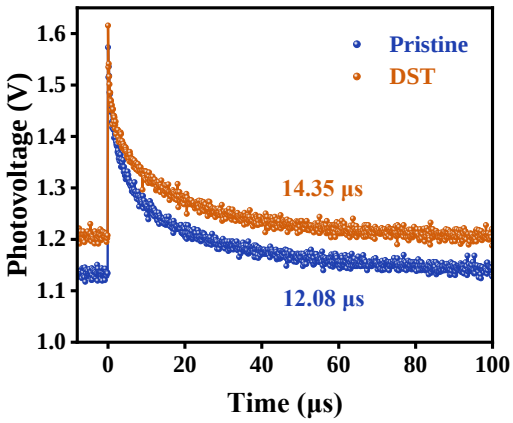

Figure S26. Transient photovoltage decay for the pristine and DST devices.

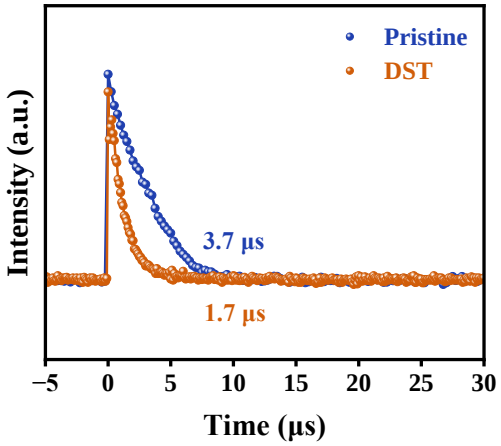

Figure S27. Normalized transient photocurrent decay for the pristine and DST devices.

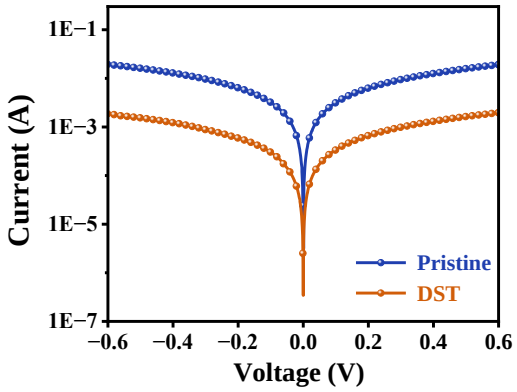

Figure S28. Dark *J-V* curves for pristine and DST devices.

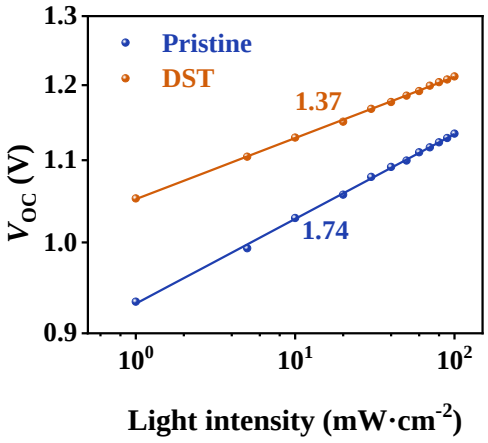

Figure S29. V_{OC} versus light intensity plots for pristine and DST devices.

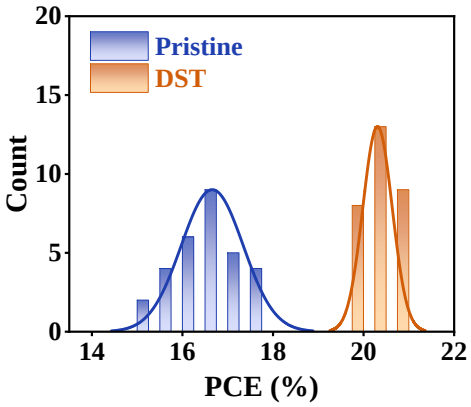

Figure S30. Statistical PCEs distribution for wide-bandgap perovskite solar cells with or without DST strategy. Thirty devices were fabricated for each batch.

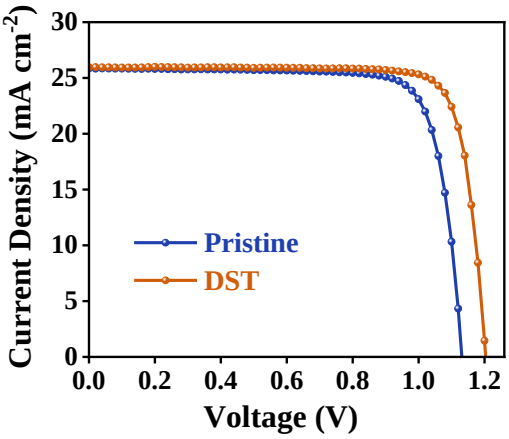

Figure S31. The initial *J*-*V* curves of corresponding devices for the ISOS-D-3 stability test.

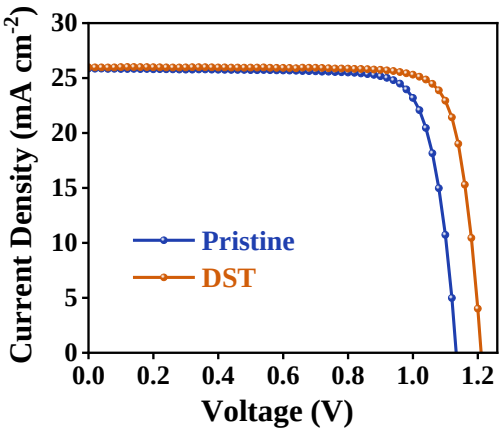

Figure S32. The initial *J-V* curves of corresponding devices for the ISOS-L-2 stability test.

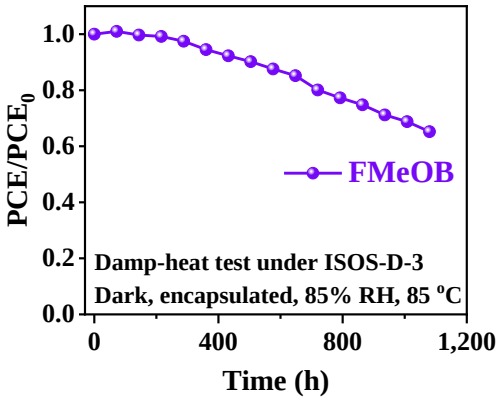

Figure S33. Damp-heat stability for the device with perovskite film post-treated by FMeOB.

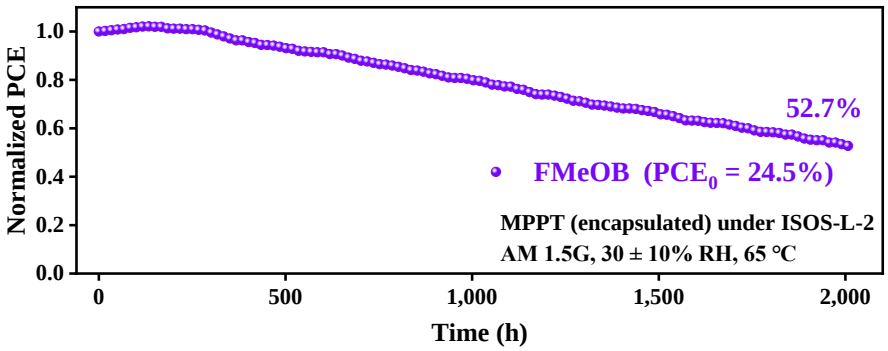

Figure S34. Maximum power point tracking of the device with perovskite film post-treated by FMeOB.

Table S1. Photovoltaic parameters of devices based Me-4PACz and perovskite films annealing at different temperature.

Annealing temperature		J_{SC} (mA cm^{-2})	V_{OC} (V)	FF (%)	PCE (%)
Me-4PACz	Perovskite				
100 ^{o}C	100 ^{o}C	25.9	1.12	80.2	23.3
100 ^{o}C	150 ^{o}C	26.0	1.06	72.3	19.9
150 ^{o}C	100 ^{o}C	25.9	1.08	70.7	19.7

Table S2. Photovoltaic parameters of the champion DST devices with FMeOB at different concentration in Figure S23a.

FMeOB Concentration	J_{SC} (mA cm^{-2})	V_{OC} (V)	FF (%)	PCE (%)
0 mg/ml	25.9	1.13	80.6	23.7
0.5 mg/ml	26.0	1.18	82.1	25.1
1.0 mg/ml	26.1	1.21	83.8	26.3
1.5 mg/ml	26.0	1.21	82.7	26.0
2.0 mg/ml	25.8	1.21	82.1	25.6

Table S3. Photovoltaic parameters of best-performing pristine and DST devices under forward and reverse scan.

		J_{SC} (mA cm^{-2})	V_{OC} (V)	FF (%)	PCE (%)	Hysteresis index (%)
Pristine	Forward	25.9	1.13	78.2	23.0	3.2
	Reverse	25.9	1.13	80.7	23.7	
DST	Forward	26.1	1.21	83.2	26.3	0.2
	Reverse	26.1	1.21	83.3	26.4	

References

1. V. W. Bergmann, Y. Guo, H. Tanaka, I. M. Hermes, D. Li, A. Klasen, S. A. Bretschneider, E. Nakamura, R. Berger and S. A. L. Weber, *ACS Appl. Mater. Interfaces*, 2016, **8**, 19402–19409.
2. Z. Ni, C. Bao, Y. Liu, Q. Jiang, W.-Q. Wu, S. Chen, X. Dai, B. Chen, B. Hartweg, Z. Yu, Z. Holman and J. Huang, *Science*, 2020, **367**, 1352–1358.
3. S. Wang, M.-H. Li, Y. Zhang, Y. Jiang, L. Xu, F. Wang and J.-S. Hu, *Energy Environ. Sci.*, 2023, **16**, 2572–2578.